Constraints on the source of reactive phases in sediment from a major Arctic river using neodymium isotopes

Christina S. Larkin[a,1]*, Alexander M. Piotrowski[a], Ruth S. Hindshaw[a,2], Germain Bayon[b], Robert G. Hilton[c], J. Jotautas Baronas[a], Mathieu Dellinger[c], Ruixue Wang[a], Edward T. Tipper[a]

Affiliations:

[a]Department of Earth Sciences, University of Cambridge, UK

[b]IFREMER, Marine Geosciences Unit, Brest, France.

[c]Department of Geography, Durham University, UK

*Corresponding author: csl42@cam.ac.uk

[1]Present address: School of Ocean and Earth Science, National Oceanography Centre, University of Southampton, UK

[2]Present address: Norconsult AS, Kjørboveien 22, 1338 Sandvika, Norway

Abstract

Riverine suspended particulate matter (SPM) is essential for the delivery of micronutrients such as iron (Fe) to the oceans. SPM is known to consist of multiple phases with differing reactivity, but their role in the delivery of elements to the oceans is poorly constrained. Here we provide new constraints on the source and composition of reactive phases in SPM from the Mackenzie River, the largest sediment source to the Arctic Ocean. Sequential leaching of SPM shows that river sediments contain labile Fe phases. We estimate the labile Fe flux is substantial (0.21(+0.06,-0.05) Tg/yr) by quantifying Fe concentrations in weak leaches of the SPM. The labile Fe phase hosts a considerable amount of rare earth elements (REE), including neodymium (Nd). We demonstrate that the labile Fe phase and dissolved load have radiogenic Nd isotope ratios that are identical within uncertainty, but up to 8 epsilon units distinct from the silicate phase. We interpret this as evidence for dynamic cycling between Fe-oxide phases in SPM and the river water, demonstrating the high reactivity of the labile Fe phase. Nd isotope and elemental molar ratios suggest that a significant amount of labile Fe- and Nd-bearing phases are derived from Fe-oxides within the sedimentary source rock rather than silicate mineral dissolution. Thus, sedimentary rock erosion and weathering provides an important source of labile Fe, manganese (Mn) and by extension potentially other trace metals. Our results imply that both past and future environmental change in the Arctic, such as permafrost thaw, may trigger changes to the supply of reactive trace metals. These results demonstrate that a re-evaluation of sediment reactivity within rivers is required where uplifted sedimentary rocks are present.

Key words: iron oxides; bioavailable; neodymium isotopes; Arctic

1. Introduction

Rivers are conduits for the transfer of particulate and dissolved material derived from weathering to the oceans (Gaillardet et al., 1999). Weathering plays a critical role in the cycling of elements at the Earth's surface and is a key regulator of the Earth's climate over geological timescales (Walker et al., 1981). Rivers also transport essential nutrients to the oceans sustaining marine primary productivity (e.g., Deutsch and Weber, 2012). Changes to the flux of nutrients that limit productivity in the oceans have been linked to large scale perturbations in the carbon cycle and past climate change (Martin, 1990; Vincent and Berger, 1985). The flux of suspended particulate matter (SPM) sustains the supply of certain elements to the oceans and plays an important role in bio-geochemical cycling (Jeandel and Oelkers, 2015; Jones et al., 2012).

Micronutrients (e.g., Fe), the rare earth elements (REE, particularly Nd) and many other trace elements have low solubility in natural waters. In the dissolved load (<0.2 μm) these elements are predominately associated with nanoparticulate and colloidal phases (Gaillardet et al., 2014, and references therein). Their concentrations in river dissolved loads are low (ppb to ppt, Gaillardet et al., 2014); concentrations in SPM are several orders of magnitude higher (Jeandel and Oelkers, 2015). Salt-induced flocculation of many such nonmobile elements in estuaries further removes most of these low concentration elements prior to reaching the oceans (Elderfield et al., 1990).

Basalts and volcanic particulates are important sources of key bio-limiting nutrients (e.g. Fe) as they are easily weatherable and enriched in those elements (Jones et al., 2012). However, the importance of sedimentary rocks has not been similarly evaluated. Marine sediments contain phases, including Fe-Mn oxyhydroxides with elevated REE concentrations, which are formed from precipitation and exchange with seawater and pore fluids (e.g., Chester and Hughes, 1967). Marine sedimentary rocks tectonically emplaced on the continents retain some of these characteristics (Hindshaw et al., 2018; Jang et al., 2020). This results in a reservoir of inherited phases which can be more reactive than silicate minerals and may supply a greater amount of bioavailable Fe to riverine sediments (Hindshaw et al., 2018). For instance, amorphous Fe (oxy)hydroxides (e.g. ferrihyrite) contained within riverine sediments are easily reducible and potentially bioavailable (Bhatia et al., 2013, Hawkings et al., 2018).

Since Fe-oxides are enriched in REEs, their origin can be traced using radiogenic Nd isotopes ($^{143}Nd/^{144}Nd$, expressed as εNd), a source tracer in riverine and marine sediments (Goldstein and Jacobsen, 1988; Goldstein and Hemming, 2003). Since there is limited fractionation of the Sm/Nd ratio in particulate phases during weathering and the decay constant is long compared to the timescales of recent weathering (Babechuk et al., 2014), εNd is only controlled by changes in source. Nd in the dissolved load typically has εNd greater (more radiogenic) than in the SPM in rivers with abundant sedimentary rocks in their catchments (Goldstein and Jacobsen, 1987; Hindshaw et al., 2018). This offset is attributed to dissolved Nd sourced from the preferential weathering of marine precipitates and other reactive components contained within the parent rock (Goldstein and Jacobsen, 1987).

Nonetheless, a clear link between these reactive phases and dissolved riverine chemistry has not been shown.

With knowledge of the source composition, εNd is a valuable tool for tracing the origin of reactive phases from sedimentary rock weathering and their transport in river systems. We apply this tracer to a large Arctic river system. The Mackenzie River, as the first and third largest source of suspended sediment and water, respectively, to the Arctic Ocean (Macdonald et al., 1998, Holmes et al., 2002), provides a good representation of basin-scale fluxes. It is dominated by shale weathering with a low abundance of volcanic or mafic rocks and limited influence from the weathering of crystalline rocks (Millot et al., 2003, Fig. 1B). This makes the Mackenzie an ideal location to investigate the mobilisation of reactive, micronutrient-bearing phases during shale weathering on a large scale.

In this study we characterize the εNd of the dissolved load (<0.2 μm and ultrafiltrates) and suspended sediment (sequential extractions and residue) in the Mackenzie and key tributaries over two years (2017, 2018) sampled within a few days of the peak discharge after ice-break up. We show that the εNd is within uncertainty between the dissolved load and easily leachable phases in the SPM. We use REE patterns to constrain the mineralogy of the leachable phases. We quantify the concentrations of major and some trace elements in leachable phases and estimate the flux of labile Fe from the Mackenzie to the Arctic Ocean.

2. Materials and Methods

126 Full analytical and procedural methods are given in Supplementary Text 1 and
127 summarised briefly here. All analysis was carried out at the University of Cambridge,
128 Department of Earth Sciences.
129
130 **2.1 Study area and sample collection**
131
132 The Mackenzie River system is large (Fig. 1, area 1.78×10^6 km^2). The weathering of
133 sedimentary rocks dominates the dissolved and SPM loads of the river (Calmels et
134 al., 2007; Horan et al., 2019; Huh et al., 2004; Millot et al., 2003) despite the large
135 surface area of crystalline rocks (29.2% of the basin geology, Fig. 1b). Less than 1%
136 of the basin is underlain by volcanic rocks (Fig. 1b). The river is characterised by a
137 sharp peak in discharge each year after the seasonal melting (freshet) of river ice in
138 May-July (Fig. 2). Samples were collected at this period of maximum flux.
139
140 The Mackenzie mainstem and two large tributaries which enter at the delta, the Peel
141 River and the Arctic Red River, were sampled at 3 main sites (Fig. 1) in early June in
142 2017 and 2018. Suspended sediment samples were taken at different depths in the
143 channel using a 5L Van-Dorn type depth sampler (following Hilton et al., 2015).
144 Discharge was quantified using an acoustic-Doppler current profiler (ADCP, Rio
145 Grande II (1200 kHz), Teledyne Instruments, Fig. 2, Supplementary Table S4).
146 Additionally, in 2018 a small Peel River tributary and meltwater from the surface
147 Arctic Ocean (seawater diluted by sea and river ice melt) were sampled. Dredged
148 bed load, bank sand and rock fragments were also collected.
149

River samples were filtered at 0.2 µm, collecting both water and sediment. Filtered waters collected for major cation and REE concentrations were acidified using distilled HNO_3 to pH 2 in acid cleaned bottles. In 2018, ultrafiltration was carried out on <0.2 µm filtrates from the Mackenzie (Middle Channel) and the Peel River, using dialysis membranes with molecular cut off weights of 10 kDa and 1 kDa (Supplementary Text 1.2). Approximately 10 L of <0.2 µm water was collected for the analysis of Nd isotopes using a Fe co-precipitation method (Hindshaw et al., 2018).

To characterize the longer-term integrated composition of the Mackenzie River SPM leachate compositions from 5 offshore sediment cores from the Mackenzie delta and one from deeper in the Beaufort Sea were analysed (Natural Resources Canada, Geology Survey of Canada's Marine Geoscience Collection, Supplementary Table S5). Two silicate residue samples were analysed from two of the shallowest core sites. The sedimentation rate at shallow sites in the Canadian Beaufort sea is high (on the order of 2-3 m/ka, O'Regan et al., 2018), indicating that the range and depth sampled within the cores (~10 cm) represents sediment that is likely several decades old, and homogenises inter-annual and seasonal variability.

2.2 Sequential extractions

Approximately 50-100 mg of dry sediment was leached sequentially to extract: 1) exchangeable phases (1M NH_4Cl), 2) reactive Fe-Mn (oxy)hyroxides (a weak acid-reductive leach of 5 mM hydroxylamine hydrochloride (HH)-3 mM Na-EDTA-1.5% acetic acid buffered to a pH of ~4 with NaOH), 3) calcite and additional carbonates (1.7M acetic acid), 4) dolomite, and any remaining authigenic components (e.g.,

crystalline Fe-Mn oxides, 1M HCl). The focus of this study is the weak acid-reductive leach, hereafter referred to as the HH leach, targeting amorphous reactive Fe-Mn oxides. This is a more dilute HH leach than previous methods (e.g. Bhatia et al., 2013; Chester and Hughes, 1967) carried out on non-decarbonated sediments, following Blaser et al., 2016. This method minimizes dissolution of silicate phases and avoids the loss of other reactive Fe phases during removal of carbonates. Due to the buffering of this reaction in the presence of varying amounts of carbonate, it represents a minimum estimate of the reactive Fe-Mn oxyhydroxides rather than a fully quantitative leach. This leach will mobilise reactive carbonate phases and potentially some REEs associated with phosphates. Residue sediment was digested following lithium borate fusion (Supplementary Text S1.3).

2.3 Major and trace concentration analysis

Major and selected trace element (e.g. Fe, Mn) concentrations on acidified waters were determined by ICP-OES (Agilent 5100, with a precision and accuracy of better than 10% based on repeated analysis of certified water standards (Supplementary Text 1.4.1).

Leachate phases and dissolved sediment residues were similarly analysed for major and some trace element concentrations by ICP-OES, with matrix-matched calibration lines. External reproducibility (typically better than 10%) was monitored using certified standards (Supplementary Text 1.4.1).

Mass balance was verified by comparison of the sum of concentrations in the leachates and residue with bulk sediment and a leached USGS shale standard with certified values (Supplementary Table 8). The sum reproduced expected values usually within 10%, and always within 20%.

2.4 REE Analysis

REE concentrations on filtered waters were measured by isotope dilution (Supplementary Text 1.5). Nd (alongside REE) concentrations in sediments and sediment leachates were determined using ICP-OES (Agilent 5100, Nd concentrations > ~4 ppb only) and using a Thermo Element-XR ICP-MS with a matrix-matched calibration line. Reproducibility was monitored using certified standards and values were within ±10%. Two residue samples and all sequential extraction steps from one SPM sample were determined by isotope dilution, as described for filtered water samples (Supplementary Text 1.5).

2.5 Nd and Sr isotopes

Nd was separated from the leachate and residue solutions using established chromatographic procedures; the light REE's were separated using TRUspec resin, and Nd from Sm using LNspec resin. Radiogenic Sr isotope ratios ($^{87}Sr/^{86}Sr$) were determined on a subset of water, sediment leachate and sediment samples. Sr was isolated using SrSpec resin (following Hindshaw et al, 2018). Nd was separated from water samples using two stages of cation exchange (Biorad AG50W-X8) and LnSpec resin (Supplementary Text 1.1).

Nd and Sr isotopes were measured on a Thermo Neptune Plus MC-ICP-MS. $^{146}Nd/^{144}Nd$ was normalised to 0.7219 using an exponential correction. Samples were corrected to the accepted value of reference standard JNdi-1; $^{143}Nd/^{144}Nd$=0.512115 (Tanaka et al., 2000) which was repeatedly analysed at the sample concentration throughout each measurement session. Two times the standard deviation (2σ) on JNdi-1 for each measurement session is quoted as the analytical uncertainty. εNd was calculated in parts per 10,000 relative to the chondritic uniform reservoir (CHUR), $^{143}Nd/^{144}Nd_{CHUR}$=0.512638 (Jacobsen and Wasserburg, 1980). For Nd isotopes, long-term reproducibility was monitored using rock standards (Supplementary Text 1.4.2). Unless otherwise stated, where Nd isotope replicates (measurement or full procedural) were carried out, the value reported is the average of the replicates and the associated 2σ, if higher than the measurement session uncertainty. For Sr isotopes, ^{85}Rb was monitored to correct for Rb interferences on ^{87}Sr and Kr interferences were corrected for by measurement of the baseline in a blank solution (on-peak zeros). Values were normalised to $^{86}Sr/^{88}Sr$ = 0.1194 using an exponential correction. For Sr isotopes, samples were analysed in duplicate, and the uncertainty quoted is the associated 2σ. Repeated measurements of the standard NBS 987 yielded $^{87}Sr/^{86}Sr$= 0.710275±46 ppm (2σ, n=20).

3. Results

3.1 Dissolved Nd

Nd was partitioned between nano-particulate and colloidal phases and the 'truly' dissolved (<1 nm; ≈1 kDa) phase (Table 1). Approximately 70% of Nd in the <0.2 μm filtrate is hosted in colloids or nano-particulates (Table 1). In the Mackenzie River (Middle Channel) εNd values between the <0.2 μm and <1 kDa fractions agreed within 0.43 epsilon units (Table 1). This demonstrates that nano-particulate and colloidal phases and the 'truly' dissolved load have the same source and so the <0.2 μm εNd value is representative of the 'truly' dissolved composition, consistent with previous observations in large rivers (Merschel et al., 2017).

3.2 Paired sediment and dissolved εNd

As the <0.2 μm fraction is indicative of the 'truly' dissolved εNd, it is possible to use these measurements to compare with leachable phases and assess their reactivity. We therefore refer to the <0.2 μm as the dissolved load. The dissolved load is always more radiogenic than the sediment residue, with the offset ranging from 1.4 to 8.2 epsilon units (Fig. 3, average = 3.2). This is consistent with, and in some cases far exceeds, the offset observed by Goldstein and Jacobsen, 1987, for large rivers with significant marine sedimentary source rocks in their catchments. In contrast, εNd in the dissolved load is in close agreement with HH leachates targeting reactive Fe-Mn oxides with a linear regression within error of the 1:1 line (Fig. 3). The dissolved vs. residue εNd linear regression is systematically offset from the 1:1 line, with a weaker correlation (Fig. 3).

Residue εNd compositions are in close agreement with previous measurements of sediment already reported for the Mackenzie River (Vonk et al., 2015). Dissolved

εNd reported herein for the Mackenzie River at Tsiigehtchic (-13.4 ±0.2 (2σ, n=1, 2018) and -12.3±0.3 (2σ, n=2, 2017)) is consistent with the only previous dissolved measurement (2003, -12.9±0.3 (Zimmermann et al., 2009)).

SPM in the Middle Channel of the Mackenzie River is hydrodynamically sorted, due to faster settling velocities of coarser sedimentary particles (e.g. Bouchez et al., 2011). This is illustrated by Al/Si, a proxy for grain size (Fig. 4), indicating the dominance of finer sediments towards the surface and coarser at the bottom. Despite this hydrodynamic sorting, there is no appreciable variation of εNd with depth in either the sediment residue or HH leachate (Fig. 4). Dissolved εNd from the surface and base of the water column demonstrate that the water is well mixed.

There are systematic differences in dissolved εNd between 2017 and 2018. The furthest downstream site (Mackenzie, Middle Channel) dissolved composition changes from εNd=-10.71±0.41 (2σ, n=3, 2017) to -12.97±0.15 (2σ, n=1, 2018), likely driven by changes in the Peel River which shows similar differences, changing from εNd=-9.83±0.16 (2σ, n=1, 2017) to -11.47±0.15 (2σ, n=1, 2018). This could represent inter-annual εNd variability, as is argued to be the case for changes in organic carbon and dissolved nutrient sources on the same sample set (Schwab et al., 2020), but additional data would be needed to determine if this is the case.

The average HH leach εNd from sediment cores was -11.3±1.9 (2σ, n=6), consistent with the same fraction in riverine sediments (Fig. 3) with the leachate always more radiogenic compared to the silicate residue (two cores, <10m deep, average offset = 2.7±1.2, 2σ, n=2). Shallow (<100 m) seawater in the Beaufort Sea is more

298 radiogenic than these leachate compositions (εNd = ~-6 to -9, Porcelli et al., 2009).
299 Therefore, the offset between residue and leachate is preserved and exported in
300 sediment to the shelf. εNd in the HH leachate at the deepest and least proximal core
301 site (εNd = -9.55, 1054 m water depth) overlaps with εNd measured in deep (> 1000
302 m) seawater in the Beaufort Sea, which is less radiogenic (εNd between -9 and -11,
303 Porcelli et al., 2009).
304
305 **3.3 Sediment partitioning and characterisation**
306
307 The partitioning of selected elements amongst all leachates relative to the bulk
308 sediment is shown in Fig. 5. In the NH_4Cl leach, targeting exchangeable phases, Fe
309 and Nd were below detection. This is consistent with a previous study which reported
310 low concentrations of REEs in a river sediment exchangeable fraction (Adebayo et
311 al., 2018). Elemental concentrations in the NH_4Cl leach which were not below
312 detection are reported in Tipper et al., 2021. The HH leach contains on average 3%,
313 8% and 30% of the total sediment Fe, Nd and Mn respectively (Fig. 5). Ca, Mg and
314 Sr are also high in the HH leach (Fig. 5) consistent with significant carbonate
315 lithologies present within the Mackenzie Basin (Millot et al., 2003). On average 60%
316 of the Fe and Nd are hosted within the silicate residue.
317
318 REE on the HH leach show a middle REE (MREE) enrichment (Fig. 6a). A MREE
319 enrichment of this magnitude is typical of an Fe-Mn oxyhydroxide signature (Fig. 6a)
320 and is consistent with that previously reported for similar sediment extractions (e.g.
321 Leybourne and Johannesson, 2008).
322

323 REE in the SPM leachate phases were partitioned relative to the bulk (sum of
324 leachates and residue; Middle Channel, 2017, Fig 6b). 15% of REEs relative to the
325 total sediment are mobilised during the HH leaching step. A smaller fraction (<1%) of
326 REEs are released during the subsequent acetic acid leach step (Fig. 6b), despite
327 the large amount of Ca and Mg (22% of total sediment Ca, 11% of total sediment
328 Mg). Less Fe and Mn are mobilised in the acetic acid leach (1% of total Fe, 5% of
329 total Mn), relative to the HH leach (4% of total Fe, 42% of total Mn). This
330 demonstrates that the REE are not associated with carbonate phases.
331
332 $^{87}Sr/^{86}Sr$ on the dissolved load and sediment residues (Fig. 6c) are in agreement
333 with previously published data for this river (e.g. Millot et al., 2003). $^{87}Sr/^{86}Sr$ values
334 indicate carbonate and silicate sources in the HH leach and residue respectively. Sr
335 isotopes do not indicate extensive leaching into the silicate detrital fraction. Although
336 there is scatter in the leachable εNd compositions (Fig. 6c), on stronger leaching εNd
337 is not substantially more radiogenic than the HH leach.
338
339 **4. Discussion**
340
341 εNd values from paired dissolved load and SPM, alongside the characterisation of
342 elemental concentrations in sequential extractions, are used to trace both the source
343 and the reactivity of different phases within the SPM. Firstly, we seek to assess the
344 reactivity of the phases in the HH leach and then characterise sources. We then
345 estimate the flux of labile Fe from the Mackenzie to the Arctic Ocean and address
346 the implications of this study in terms of the oceanic Nd budget.
347

348 **4.1 Reactivity of the labile phases in SPM**

349

350 The reactivity of phases hosted in the HH leachate are traced with εNd and
351 elemental partitioning. Significant fractions of Fe, Mn, Ca, Mg, and REEs relative to
352 the bulk sediment are present in what is an extremely weak and buffered leach (5
353 mM HH, 1.5% acetic acid, Fig. 5, Fig. 6). Although subsequent leaches use stronger
354 reactants and are not buffered, they release smaller amounts of Nd compared to the
355 HH leach (Fig. 6b). This suggests that some of these reactive phases are
356 susceptible to acid-reductive dissolution with small changes in pH or redox
357 conditions (which may occur in the delta or offshore). Nd and REEs are depleted in
358 carbonate rocks and are unlikely to be directly incorporated into biogenic calcite (e.g.
359 Tachikawa et al., 2014). Less Nd is released in the 1.7 M acetic acid leach,
360 compared to the HH leach, confirming that during the HH leaching step the Nd
361 released is not associated with carbonates.

362

363 Although an MREE enrichment in the HH leach is typical of an Fe-Mn oxyhydroxide
364 phase, this could also be consistent with some phosphate phases (such as biogenic
365 apatite, Fig. 6a., Leybourne and Johannesson, 2008, and references therein).
366 Secondary precipitation of phosphates could also result in an MREE enrichment
367 (Leybourne and Johannesson, 2008), but the lack of an LREE enrichment (low
368 HREE/LREE, Fig. 6a) in HH leaches makes this unlikely (Köhler et al., 2005).

369

370 The dissolved εNd composition is always similar to the HH leachate composition
371 (Fig. 3). This similarity is prevalent in different sampling localities and tributaries,
372 which differ in sediment and water characteristics. This points to a fundamental

process that is shared between these catchments and suggests that this observation is not unique to the time of year sampled (freshet). In rivers, the SPM is supplied by bank erosion and hillslope processes (Hilton et al., 2015), which are likely to be decoupled in space and time from the hydrological pathways that deliver river water (Vonk et al., 2019). Therefore, the consistency in εNd between dissolved and HH leach εNd is most likely explained by rapid and recent cycling within riverine implying equilibrium between the dissolved load and Fe-oxide phases in the HH leach.

Dissolved and HH leachate εNd are always similar at each site in the Mackenzie River, both upstream and downstream of major confluences with the Peel and Arctic Red Rivers (Tsiigehtchic to Middle Channel, Fig. 1a). Previous discharge and sediment flux estimates demonstrate that water and suspended sediment do not mix in the same proportions downstream of the Peel confluence, with the Peel supplying 17% of the sediment load (Carson et al., 1998), but only 7% of the total water discharge (Schwab et al., 2020 and references therein). This implies the potential for rapid cycling between the dissolved load and HH leach phases during transit between the upstream and downstream sites, despite only limited changes in pH and Nd concentration (supplementary Table S4 and S10).

Although the mechanism for equilibration of Nd between HH leach phases and the dissolved load is unclear, since the weakly adsorbed exchangeable phases are removed in the leaching step prior to the HH leach, this rapid cycling is likely driven by dissolution of Nd from phases such as Fe-Mn oxyhydroxides. The concentration of Nd in the HH leach (ppb to ppm, Supplementary Table S9 and S11) is several orders of magnitude higher than the dissolved concentration (Supplementary Table

S10), suggesting that phases within the HH leach may drive the dissolved composition.

Our findings demonstrate dynamic cycling between the dissolved load and phases soluble in the HH leach, such as Fe-Mn oxyhydroxides. The similarity of the dissolved load and HH leach phases and decoupling from the silicate residue suggests that the HH leach phases are labile and likely bioavailable. These results imply not only rapid cycling of Nd but potentially other immobile elements contained within the HH leach.

4.2 Marine authigenic phases as a source of radiogenic Nd in river waters

The mass balance of sources of radiogenic Nd that contribute to higher εNd in the dissolved and HH fractions relative to silicates provides information on the relative supply of Nd from different phases. Here we discuss possible sources of radiogenic Nd that could explain both the HH leaches and dissolved load. Average global seawater εNd (~-8.8, Lacan et al., 2012) and modern core top authigenic fractions (Haley et al., 2017) are more radiogenic than the upper continental crust (-11.4±2.5, Goldstein et al., 1984). Therefore, when marine sediments are emplaced on the continents, they can provide a distinct source of radiogenic Nd to the weathering reactor. Measurements of εNd on Fe-Mn oxides and other inherited authigenic phases of marine origin hosted in sedimentary rocks show that they are on average more radiogenic than associated silicates (Jang et al., 2020, Hindshaw et al., 2018). They can be reactive and so result in a more radiogenic dissolved and leachate

422 composition when compared to the bulk source rock in rivers (Bayon et al., 2020;
423 Goldstein and Jacobsen, 1987; Hindshaw et al., 2018; Jang et al., 2020).
424
425 Preferential weathering of inherited marine authigenic phases is the most likely
426 reason for decoupled εNd between dissolved and silicate residue sediment in the
427 Mackenzie. Radiogenic Nd in Fe-Mn oxyhydroxides of Mackenzie River SPM is likely
428 derived from the weathering of these phases through physical transportation, and
429 equilibration with waters. These radiogenic phases become mixed with Fe-oxides
430 resulting from the weathering of silicate minerals, with εNd inherited from the source
431 silicate. Nonetheless, it is possible that alternate sources contribute labile and
432 radiogenic Nd, and these are addressed below.
433
434 **4.3 Alternative sources of radiogenic Nd to river waters**
435 Accessory minerals enriched in REEs and garnet can have more radiogenic εNd
436 than their bulk source rocks (e.g. Rickli et al., 2017). However, radiogenic release of
437 Nd during incongruent weathering of crystalline rocks is minimal (Dausmann et al.,
438 2019). Another possible source of radiogenic Nd is the preferential weathering of
439 volcanic rocks, but they are rare in the Mackenzie basin (Fig 1b, Millot et al., 2003).
440
441 Several studies indicate the dominance of shale and carbonate weathering on the
442 Mackenzie dissolved load, with no evidence of large volcanic or crystalline rock
443 contributions (Horan et al., 2019; Huh et al., 2004; Millot et al., 2003). εNd
444 decoupling between dissolved and silicate residue is at a maximum in a small Peel
445 River tributary that, to the best of our knowledge, does not have crystalline or
446 volcanic rocks in its catchment and drains almost exclusively shales. Moreover,

447 preferential weathering of a specific rock type would not explain the coupling of the
448 dissolved load with the HH leach, and their decoupling from the silicate residue, in all
449 sampling sites, with differing source lithologies.
450 Phosphates in sedimentary rocks are enriched in REEs and may be partially
451 mobilised in the HH leach. Phosphates in the main source rock type (shales) are
452 likely to have formed during marine diagenesis, so can be considered as inherited
453 authigenic phases, with a comparable εNd to concurrent Fe-Mn oxides. Fe-oxides
454 are ubiquitous in all sediments and sedimentary rocks. Given the range in source
455 rock age (Proterozoic to Cenozoic, Wheeler, 1996) and depositional environment,
456 Fe-Mn oxides are the most probable universal constituent consistent with the high
457 fraction of Fe and Mn in the HH leach, whereas phosphates may not always be
458 present in sufficient abundance. Equilibration between the dissolved load and
459 phosphates hosted in the HH leach would not likely result in the observed REE
460 patterns, as secondary phosphates are typically LREE enriched (Fig. 6a, Köhler et
461 al., 2005). Therefore, it is unlikely that phosphate minerals play a significant role, and
462 the more positive Nd is derived from the preferential weathering of inherited Fe-Mn
463 oxides.
464
465 While Fe-Mn oxides are insoluble in oxygenated and neutral range pH which typify
466 large rivers including the Mackenzie (Tank et al., 2016) mobilization of amorphous
467 and nano-particulate Fe can occur, and in acidic environments dissolution of Fe-
468 oxides may occur. Extensive pyrite oxidation provides the majority of dissolved
469 sulfate in the Mackenzie (Calmels et al., 2007). A product of the oxidative weathering
470 of pyrite is Fe-oxide, and if instantaneous buffering of this reaction by dissolution of
471 carbonate minerals does not occur, it will result in an acidic pH alongside high sulfate

concentrations (Horan et al., 2019). This is seen in one tributary of the Peel River where high sulfate concentrations (4660 μM) and relatively low pH of ~6 are coupled to elevated Nd (950 ppt), high Fe (1 μM) and Mn (7.8 μM) concentrations in the dissolved load (<0.2 μm, Supplementary Tables S9 and S12) with the highest observed offset between the residue and HH leach εNd (8 epsilon units, Supplementary Table S10).

Nd is not likely to be incorporated directly into pyrite but will be present in 'contaminant' phases in pyrite or in other phases within a sedimentary rock succession, namely Fe-Mn oxyhydroxides or phosphates (Raiswell and Plant, 1980). High Nd and Mn dissolved concentrations indicate the dissolution of reactive Fe-Mn oxides within the source rock (shale), with differing εNd to silicate sources, coupled to the oxidative weathering of pyrite.

The HH leach of a shale fragment from this catchment has comparable εNd to the bedload HH leachate and dissolved load (Fig. 3, Supplementary Table S10). Although the mineralogical source of Nd and Fe is different (Fe from pyrite and Nd from other phases) these observations imply that the mobilization of Fe and Nd are coupled during the oxidative weathering of pyrite. This suggests that oxidative weathering of pyrite may provide an important source of reactive Nd and Fe bearing phases, with radiogenic εNd. Once the REEs are in solution, they can be incorporated into secondary Fe-oxides upon increasing pH, when Fe-oxides bearing REEs will precipitate out of solution. Close coupling between riverine Nd and Fe has been noted in previous studies (e.g. Elderfield et al., 1990; Ingri et al., 2000).

4.4 Constraints on the contribution of different sources of labile Fe and Nd

Using a simple mass balance model it is possible to estimate the fraction of Nd and Fe sourced from inherited authigenic phases contained within the sedimentary source rocks.

Dissolved εNd is set by exchange with labile HH leach phases in the SPM. The labile εNd is considered to be a mixture of Fe-oxides derived from modern-day weathering of silicate minerals (εNd_{sil}) and Nd derived from inherited authigenic phases (εNd_{auth}, equation 1, Figure 7).

$$\varepsilon Nd_{labile} = f_{Nd,auth}\varepsilon Nd_{auth} + f_{Nd,sil}\varepsilon Nd_{sil} \quad (1)$$

where εNd_{labile} is the average of the leachate and dissolved composition, and f is the fraction of Nd in either the inherited authigenic or silicate phases where $f_{Nd,auth} + f_{Nd,sil} = 1$.

Equation 1 was solved for $f_{Nd,auth}$, with εNd_{sil} given by the residue silicate composition measured for sample set. εNd_{labile} is the average of the HH leachate composition and (if measured) the dissolved composition for each sample set. εNd_{auth} is unknown and given the range of ages and types of sedimentary rocks in the Mackenzie basin, will be variable. εNd_{auth} was considered over the range $\varepsilon Nd_{auth}=0$ to $\varepsilon Nd_{auth}= \varepsilon Nd_{labile}$ sampled from a synthetic uniform distribution to account for the uncertainty of this end-member. εNd_{labile} and εNd_{sil} were measured at each sampling location and considered as normal distributions. We used Monte-Carlo methods to estimate the error when solving for $f_{Nd,auth}$ (calculating $f_{Nd,auth}$ for 100,000 values of each variable). $f_{Nd,auth}$ was calculated for 4 individual sample sets (2017 and 2018 Middle Channel,

Arctic Ocean and in shelf sediment cores, Fig. 8, Supplementary Table S13). Taking the interquartile range from the sum of all four sample sets it estimated that, at the mouth of the Mackenzie River a minimum of 23-50% of labile Nd is derived from inherited authigenic phases (Fig. 8).

Given this significant estimate for $f_{Nd,auth}$, it is likely that a similarly high fraction of other immobile elements such are Fe are also sourced from inherited authigenic phases. The fraction of labile Fe sourced from inherited authigenic phases (including from pyrite and inherited Fe-oxides) was estimated using mass balance:

$$\left(\frac{Nd}{Fe}\right)_{labile} = f_{Fe,sil}\left(\frac{Nd}{Fe}\right)_{sil} + f_{Fe,auth}\left(\frac{Nd}{Fe}\right)_{auth} \quad (2)$$

where $f_{Fe,auth} + f_{Fe,sil} = 1$, and $\left(\frac{Nd}{Fe}\right)_i$ is the molar ratio of Nd to Fe in each phase. This equation was solved for $f_{Fe,auth}$, the fraction of labile Fe sourced from inherited authigenic phases. $\left(\frac{Nd}{Fe}\right)_{auth}$ is unknown, and the largest source of error and was based on the range from HH leaches of a shale fragment and coarse bank sediment ($\left(\frac{Nd}{Fe}\right)$ x 1000 = 0.63 to 2.4). $\left(\frac{[Nd]}{[Fe]}\right)_{sil}$ was taken as the average of the measured silicate residue values which are within error of average upper continental crustal estimates ($\left(\frac{Nd}{Fe}\right)$ x 1000 = 0.33±0.1, Supplementary Text 3). $\left(\frac{Nd}{Fe}\right)_{labile}$ is the measured HH leachate composition at each sampling site. Using Monte Carlo methods to estimate errors, $f_{Fe,auth}$ is estimated to be between 11-29% (interquartile range, from sum of Middle Channel samples sets, 2017 and 2018, Supplementary Table S14).

Despite the uncertainty it is clear that the SPM in the Mackenzie must host a significant fraction of labile Nd and Fe which is derived from inherited authigenic

phases in sedimentary rocks. Accordingly, the weathering of sedimentary rocks, especially marine shales, must supply a significant amount of reactive immobile elements (Nd, Fe) in the Mackenzie basin.

4.5 The flux of labile, potentially bioavailable, Fe

We have demonstrated that the SPM in the Mackenzie River has a labile Fe phase. To estimate its supply to the Arctic Ocean, we use the suspended sediment flux, which is well documented for the Mackenzie in the years 1974-1994. There is significant inter-annual variability ranging from 81 Tg/yr to 224 Tg/yr (Carson et al., 1998) with a consistent seasonal peak in the summer months following freshet, the time period over which our samples were collected (Fig. 2).

The labile, potentially bioavailable, Fe concentration was considered to be equal to the HH leach Fe concentration measured on SPM from the Mackenzie (Middle Channel, 2017 and 2018), which approximated to a normal distribution (1466±350 μg/g (±1σ, n=16)). The uncertainty was estimated using Monte-Carlo methods (n=100000), similar to that used by Hilton et al., 2015. The sediment flux was considered as a uniform distribution, taking into account all potential values at equal probability (81 Tg/yr to 224 Tg/yr, Carson et al., 1998), a maximum approximation of error. The median (±interquartile range) flux of labile Fe associated with SPM in the Mackenzie River was calculated to be 0.21(+0.06,-0.05) Tg/yr. We do not include dissolved (<0.2 μm) Fe concentrations in this estimate as they are negligible in comparison to Fe hosted in the reactive sediment phase (estimated dissolved Fe flux represents <0.03% of the labile sediment Fe flux, Supplementary Text 4).

The calculated flux of potentially bioavailable Fe in the SPM of the Mackenzie is substantial; comparable to that from the Greenland Ice Sheet (~0.3 Tg/yr, Bhatia et al., 2013). Greenland Ice Sheet fluxes are estimated using the sum of strong SPM leaching and dissolved Fe followed by the application of an estuarine loss factor (90%, Bhatia et al., 2013).

Much of the SPM from the Mackenzie is rapidly buried offshore or trapped in the delta, and the loss due to estuarine processes is unknown. Even if ~90% of the bioavailable Fe in the SPM is removed or trapped, the resulting flux to the oceans is still significant (~0.02 Tg/yr). Moreover, benthic release of this particulate associated Fe, alongside Nd, on the Mackenzie shelf may play an important role in delivering a higher proportion of this labile phase to the Arctic Ocean.

For every two moles of sulfate released from the oxidative weathering of pyrite in the Mackenzie basin, 1 mole of Fe will be incorporated into an Fe-oxide. Using the pyrite-derived sulfate flux of Calmels et al., 2007 it is estimated that the oxidative weathering of pyrite will result in the production of ~3.6 Tg/yr of Fe, as Fe-oxides. This is around an order of magnitude greater than the labile Fe flux associated with SPM that we estimate herein (0.2 Tg/yr). This implies a large accumulation of Fe-oxides derived from the oxidative weathering of pyrite within the critical zone in the Mackenzie basin, which are not exported to labile phases in the SPM.

4.6 Nd isotopic end-member compositions and inputs to the Arctic ocean

595 The Mackenzie River is a large point source of sediment and water to the Arctic
596 Ocean; therefore, it is an important finding that labile Nd has an isotopic composition
597 that is distinct from the bulk SPM. This finding is potentially applicable to all riverine
598 catchments with marine sedimentary source rocks. It is equally noteworthy that there
599 is variability in dissolved εNd between sampling years. Although our data is similar to
600 the only previous dissolved data point on the Mackenzie (Zimmermann et al., 2009),
601 it extends the range with implications for studies involving εNd in the Arctic Ocean
602 (e.g. Deschamps et al., 2019). Despite variability the HH leachates from shallow
603 marine core sites reflect the average dissolved composition of the Mackenzie over
604 decadal timescales. Therefore, such leachates from shelf sediment may provide a
605 more useful integrated εNd end-member. This isotopically distinct, labile, phase is
606 maintained offshore, meaning that any labelling of seawater via 'boundary exchange'
607 processes on the shelf will have a significantly more radiogenic composition than the
608 bulk sediment. This suggests that bulk shelf sediment and continental margin εNd
609 may be systematically offset from the likely oceanic source (Jeandel et al., 2007) as
610 it is the reactive (leachable) compositions which will characterise any shelf inputs.
611
612 **5 Conclusions**
613
614 This study highlights the potential for sedimentary rock weathering in the Arctic to
615 provide a critical source of labile Fe. As approximately half of the rocks weathered on
616 land draining into the Arctic Ocean are shales (Amiotte Suchet et al., 2003), similar
617 observations to this study would be expected in other Arctic rivers. The on-going
618 state of permafrost thaw in the Mackenzie basin has resulted in increased slumping
619 in the Peel catchment which has exposed fresh pyrite minerals and resulted in

increased sulfuric acid weathering (Zolkos et al., 2018). Increased exposure of pyrite may also lead to increased mobility and dissolution of REEs (and Fe) within this catchment. However, it is also important to note that delivery of bioavailable Fe from the Mackenzie basin to the Arctic Ocean will have changed in the past, including during periods of glaciation and glacial retreat in this region. Melt water and ice-rafting could have allowed for more direct delivery of un-weathered labile Fe phases to the Arctic Ocean.

Recycled sedimentary components within source rocks may provide labile micronutrients and other trace elements, a process which is likely applicable globally, and not just in the Arctic. Fe, and the supply of other micronutrients that limit primary productivity, are thought to be capable of having long-term and far-reaching effects on global climate, by way of their potential for increasing productivity and organic carbon burial in the oceans. Therefore, when considering increases in nutrient availability in the past, the source lithology and its reactivity must be taken into consideration. We highlight the impact of source lithology on the budget of labile trace elements (Nd) and micronutrients (Fe) in rivers, which has implications for both present and past fluxes to the oceans and paves the way for restructuring how riverine SPM is viewed in terms of its reactivity when sedimentary rocks are present in the source catchment.

Acknowledgements

M. Greaves, G. Hughes, H. Chapman, M. Bickle and K. Relph are thanked for their assistance in the lab. E. Amos and M. Schwab are thanked for assisting with

fieldwork. E. Stevenson is thanked for her help and advice on Arctic fieldwork and the co-precipitation method. M. Murphy and C. Arendt are thanked for sharing their methods for ultra-filtration and $FeCl_3$ cleaning respectively. Y. Plancherel and E. Stevenson are thanked for supplying filtered Severn River water used as an internal standard. K. Jarrett and the Geological Survey of Canada, Marine Geoscience Collection are thanked for supplying sediment core subsamples. The authors both thank and acknowledge the assistance of the Aurora College Research Institute, Inuvik. Samples were collected under research licenses 15288 and 16106. C.S.L was funded by a NERC studentship (NE/L002507/1) with support for travel to Canada in 2018 from the University of Cambridge Department of Earth Sciences Leave to Work Away Research Fund. R.G.H acknowledges funding from the European Research Council (Starting Grant ROC-CO_2, 678779) and a NERC UK-Canada Arctic Partnership Bursaries Program. E.T.T acknowledges funding from NERC Standard Grant 703 NE/P011659/1. The manuscript was greatly improved by comments from two helpful anonymous reviewers and the editor L. Derry.

References

Adebayo, S.B., Cui, M., Hong, T., White, C.D., Martin, E.E., Johannesson, K.H., 2018. Rare Earth Elements Geochemistry and Nd Isotopes in the Mississippi River and Gulf of Mexico Mixing Zone. Front. Mar. Sci. 5. https://doi.org/10.3389/fmars.2018.00166

Amiotte Suchet, P., Probst, J.-L., Ludwig, W., 2003. Worldwide distribution of continental rock lithology: Implications for the atmospheric/soil CO2 uptake by continental weathering and alkalinity river transport to the oceans. Glob. Biogeochem. Cycles 17. https://doi.org/10.1029/2002GB001891

Babechuk, M.G., Widdowson, M., Kamber, B.S., 2014. Quantifying chemical weathering intensity and trace element release from two contrasting basalt profiles, Deccan Traps, India. Chem. Geol. 363, 56–75. https://doi.org/10.1016/j.chemgeo.2013.10.027

Bayon, G., Lambert, T., Vigier, N., De Deckker, P., Freslon, N., Jang, K., Larkin, C.S., Piotrowski, A.M., Tachikawa, K., Thollon, M., Tipper, E.T., 2020. Rare earth element and neodymium isotope tracing of sedimentary rock weathering. Chem. Geol. 119794. https://doi.org/10.1016/j.chemgeo.2020.119794

Bhatia, M.P., Kujawinski, E.B., Das, S.B., Breier, C.F., Henderson, P.B., Charette, M.A., 2013. Greenland meltwater as a significant and potentially bioavailable source of iron to the ocean. Nat. Geosci. 6, 274–278. https://doi.org/10.1038/ngeo1746

Blaser, P., Lippold, J., Gutjahr, M., Frank, N., Link, J.M., Frank, M., 2016. Extracting foraminiferal seawater Nd isotope signatures from bulk deep sea sediment by chemical leaching. Chem. Geol. 439, 189–204. https://doi.org/10.1016/j.chemgeo.2016.06.024

Bouchez, J., Gaillardet, J., France- Lanord, C., Maurice, L., Dutra- Maia, P., 2011. Grain size control of river suspended sediment geochemistry: Clues from Amazon River depth profiles. Geochem. Geophys. Geosystems 12. https://doi.org/10.1029/2010GC003380

Calmels, D., Gaillardet, J., Brenot, A., France-Lanord, C., 2007. Sustained sulfide oxidation by physical erosion processes in the Mackenzie River basin: Climatic perspectives. Geology 35, 1003. https://doi.org/10.1130/G24132A.1

694 Carson, M.A., Jasper, J.N., Conly, F.M., 1998. Magnitude and Sources of Sediment
695 Input to the Mackenzie Delta, Northwest Territories, 1974–94. Arctic 51, 116–
696 124. https://doi.org/10.14430/arctic1053
697 Chester, R., Hughes, M.J., 1967. A chemical technique for the separation of ferro-
698 manganese minerals, carbonate minerals and adsorbed trace elements from
699 pelagic sediments. Chem. Geol. 2, 249–262. https://doi.org/10.1016/0009-
700 2541(67)90025-3
701 Dausmann, V., Gutjahr, M., Frank, M., Kouzmanov, K., Schaltegger, U., 2019.
702 Experimental evidence for mineral-controlled release of radiogenic Nd, Hf and
703 Pb isotopes from granitic rocks during progressive chemical weathering.
704 Chem. Geol. 507, 64–84. https://doi.org/10.1016/j.chemgeo.2018.12.024
705 Deschamps, C.-E., Montero- Serrano, J.-C., St- Onge, G., Poirier, A., 2019.
706 Holocene Changes in Deep Water Circulation Inferred From Authigenic Nd
707 and Hf Isotopes in Sediment Records From the Chukchi-Alaskan and
708 Canadian Beaufort Margins. Paleoceanogr. Paleoclimatology 34, 1038–1056.
709 https://doi.org/10.1029/2018PA003485
710 Deutsch, C., Weber, T., 2012. Nutrient Ratios as a Tracer and Driver of Ocean
711 Biogeochemistry. Annu. Rev. Mar. Sci. 4, 113–141.
712 https://doi.org/10.1146/annurev-marine-120709-142821
713 Elderfield, H., Upstill-Goddard, R., Sholkovitz, E.R., 1990. The rare earth elements in
714 rivers, estuaries, and coastal seas and their significance to the composition of
715 ocean waters. Geochim. Cosmochim. Acta 54, 971–991.
716 https://doi.org/10.1016/0016-7037(90)90432-K

717 Gaillardet, J., Dupré, B., Louvat, P., Allègre, C.J., 1999. Global silicate weathering
718 and CO2 consumption rates deduced from the chemistry of large rivers.
719 Chem. Geol. 159, 3–30. https://doi.org/10.1016/S0009-2541(99)00031-5
720 Gaillardet, J., Viers, J., Dupré, B., 2014. 7.7 - Trace Elements in River Waters, in:
721 Holland, H.D., Turekian, K.K. (Eds.), Treatise on Geochemistry (Second
722 Edition). Elsevier, Oxford, pp. 195–235. https://doi.org/10.1016/B978-0-08-
723 095975-7.00507-6
724 Goldstein, S.J., Jacobsen, S.B., 1988. Nd and Sr isotopic systematics of river water
725 suspended material: implications for crustal evolution. Earth Planet. Sci. Lett.
726 87, 249–265. https://doi.org/10.1016/0012-821X(88)90013-1
727 Goldstein, S.J., Jacobsen, S.B., 1987. The Nd and Sr isotopic systematics of river-
728 water dissolved material: Implications for the sources of Nd and Sr in
729 seawater. Chem. Geol. Isot. Geosci. Sect. 66, 245–272.
730 https://doi.org/10.1016/0168-9622(87)90045-5
731 Goldstein, S.L., Hemming, S.R., 2003. Long-lived isotopic tracers in oceanography,
732 paleoceanography, and ice-sheet dynamics. Treatise Geochem. 6, 453–489.
733 Goldstein, S.L., O'Nions, R.K., Hamilton, P.J., 1984. A Sm-Nd isotopic study of
734 atmospheric dusts and particulates from major river systems. Earth Planet.
735 Sci. Lett. 70, 221–236. https://doi.org/10.1016/0012-821X(84)90007-4
736 Haley, B.A., Du, J., Abbott, A.N., McManus, J., 2017. The Impact of Benthic
737 Processes on Rare Earth Element and Neodymium Isotope Distributions in
738 the Oceans. Front. Mar. Sci. 4. https://doi.org/10.3389/fmars.2017.00426
739 Hawkings, J.R., Benning, L.G., Raiswell, R., Kaulich, B., Araki, T., Abyaneh, M.,
740 Stockdale, A., Koch-Müller, M., Wadham, J.L., Tranter, M., 2018. Biolabile

741 ferrous iron bearing nanoparticles in glacial sediments. Earth Planet. Sci. Lett.
742 493, 92–101. https://doi.org/10.1016/j.epsl.2018.04.022
743 Hilton, R.G., Galy, V., Gaillardet, J., Dellinger, M., Bryant, C., O'Regan, M., Gröcke,
744 D.R., Coxall, H., Bouchez, J., Calmels, D., 2015. Erosion of organic carbon in
745 the Arctic as a geological carbon dioxide sink. Nature 524, 84–87.
746 https://doi.org/10.1038/nature14653
747 Hindshaw, R.S., Aciego, S.M., Piotrowski, A.M., Tipper, E.T., 2018. Decoupling of
748 dissolved and bedrock neodymium isotopes during sedimentary cycling.
749 Geochem. Perspect. Lett. 43–46. https://doi.org/10.7185/geochemlet.1828
750 Holmes, R.M., McClelland, J.W., Peterson, B.J., Shiklomanov, I.A., Shiklomanov,
751 A.I., Zhulidov, A.V., Gordeev, V.V., Bobrovitskaya, N.N., 2002. A circumpolar
752 perspective on fluvial sediment flux to the Arctic ocean. Glob. Biogeochem.
753 Cycles 16, 1098. https://doi.org/10.1029/2001GB001849
754 Horan, K., Hilton, R.G., Dellinger, M., Tipper, E., Galy, V., Calmels, D., Selby, D.,
755 Gaillardet, J., Ottley, C.J., Parsons, D.R., Burton, K.W., 2019. Carbon dioxide
756 emissions by rock organic carbon oxidation and the net geochemical carbon
757 budget of the Mackenzie River Basin. Am. J. Sci. 319, 473–499.
758 https://doi.org/10.2475/06.2019.02
759 Huh, Y., Birck, J.-L., Allègre, C.J., 2004. Osmium isotope geochemistry in the
760 Mackenzie River basin. Earth Planet. Sci. Lett. 222, 115–129.
761 https://doi.org/10.1016/j.epsl.2004.02.026
762 Ingri, J., Widerlund, A., Land, M., Gustafsson, Ö., Andersson, P., Öhlander, B., 2000.
763 Temporal variations in the fractionation of the rare earth elements in a boreal
764 river; the role of colloidal particles. Chem. Geol. 166, 23–45.
765 https://doi.org/10.1016/S0009-2541(99)00178-3

766 Jacobsen, S.B., Wasserburg, G.J., 1980. Sm-Nd isotopic evolution of chondrites.
767 Earth Planet. Sci. Lett. 50, 139–155. https://doi.org/10.1016/0012-
768 821X(80)90125-9
769 Jang, K., Bayon, G., Han, Y., Joo, Y.J., Kim, Ji-Hoon, Ryu, J.-S., Woo, J., Forwick,
770 M., Szczuciński, W., Kim, Jung-Hyun, Nam, S.-I., 2020. Neodymium isotope
771 constraints on chemical weathering and past glacial activity in Svalbard. Earth
772 Planet. Sci. Lett. 542, 116319. https://doi.org/10.1016/j.epsl.2020.116319
773 Jeandel, C., Arsouze, T., Lacan, F., Téchiné, P., Dutay, J.-C., 2007. Isotopic Nd
774 compositions and concentrations of the lithogenic inputs into the ocean: A
775 compilation, with an emphasis on the margins. Chem. Geol. 239, 156–164.
776 https://doi.org/10.1016/j.chemgeo.2006.11.013
777 Jeandel, C., Oelkers, E.H., 2015. The influence of terrigenous particulate material
778 dissolution on ocean chemistry and global element cycles. Chem. Geol. 395,
779 50–66. https://doi.org/10.1016/j.chemgeo.2014.12.001
780 Jones, M.T., Pearce, C.R., Oelkers, E.H., 2012. An experimental study of the
781 interaction of basaltic riverine particulate material and seawater. Geochim.
782 Cosmochim. Acta 77, 108–120. https://doi.org/10.1016/j.gca.2011.10.044
783 Köhler, S.J., Harouiya, N., Chaïrat, C., Oelkers, E.H., 2005. Experimental studies of
784 REE fractionation during water–mineral interactions: REE release rates during
785 apatite dissolution from pH 2.8 to 9.2. Chem. Geol. 222, 168–182.
786 https://doi.org/10.1016/j.chemgeo.2005.07.011
787 Lacan, F., Tachikawa, K., Jeandel, C., 2012. Neodymium isotopic composition of the
788 oceans: A compilation of seawater data. Chem. Geol. 300–301, 177–184.
789 https://doi.org/10.1016/j.chemgeo.2012.01.019

790 Leybourne, M.I., Johannesson, K.H., 2008. Rare earth elements (REE) and yttrium
791 in stream waters, stream sediments, and Fe–Mn oxyhydroxides:
792 Fractionation, speciation, and controls over REE+Y patterns in the surface
793 environment. Geochim. Cosmochim. Acta 72, 5962–5983.
794 https://doi.org/10.1016/j.gca.2008.09.022
795 Macdonald, R.W., Solomon, S.M., Cranston, R.E., Welch, H.E., Yunker, M.B.,
796 Gobeil, C., 1998. A sediment and organic carbon budget for the Canadian
797 Beaufort Shelf. Mar. Geol. 144, 255–273. https://doi.org/10.1016/S0025-
798 3227(97)00106-0
799 Martin, E.E., Blair, S.W., Kamenov, G.D., Scher, H.D., Bourbon, E., Basak, C.,
800 Newkirk, D.N., 2010. Extraction of Nd isotopes from bulk deep sea sediments
801 for paleoceanographic studies on Cenozoic time scales. Chem. Geol. 269,
802 414–431. https://doi.org/10.1016/j.chemgeo.2009.10.016
803 Martin, J.H., 1990. Glacial-interglacial CO2 change: The Iron Hypothesis.
804 Paleoceanography 5, 1–13. https://doi.org/10.1029/PA005i001p00001
805 Merschel, G., Bau, M., Schmidt, K., Münker, C., Dantas, E.L., 2017. Hafnium and
806 neodymium isotopes and REY distribution in the truly dissolved,
807 nanoparticulate/colloidal and suspended loads of rivers in the Amazon Basin,
808 Brazil. Geochim. Cosmochim. Acta 213, 383–399.
809 https://doi.org/10.1016/j.gca.2017.07.006
810 Millot, R., Gaillardet, J. érôme, Dupré, B., Allègre, C.J., 2003. Northern latitude
811 chemical weathering rates: clues from the Mackenzie River Basin, Canada.
812 Geochim. Cosmochim. Acta 67, 1305–1329. https://doi.org/10.1016/S0016-
813 7037(02)01207-3

O'Regan, M., Coxall, H., Hill, P., Hilton, R., Muschitiello, F., Swärd, H., 2018. Early Holocene sea level in the Canadian Beaufort Sea constrained by radiocarbon dates from a deep borehole in the Mackenzie Trough, Arctic Canada. Boreas 47, 1102–1117. https://doi.org/10.1111/bor.12335

Porcelli, D., Andersson, P.S., Baskaran, M., Frank, M., Björk, G., Semiletov, I., 2009. The distribution of neodymium isotopes in Arctic Ocean basins. Geochim. Cosmochim. Acta 73, 2645–2659. https://doi.org/10.1016/j.gca.2008.11.046

Pourmand, A., Dauphas, N., Ireland, T.J., 2012. A novel extraction chromatography and MC-ICP-MS technique for rapid analysis of REE, Sc and Y: Revising CI-chondrite and Post-Archean Australian Shale (PAAS) abundances. Chem. Geol. 291, 38–54. https://doi.org/10.1016/j.chemgeo.2011.08.011

Raiswell, R., Plant, J., 1980. The incorporation of trace elements into pyrite during diagenesis of black shales, Yorkshire, England. Econ. Geol. 75, 684–699. https://doi.org/10.2113/gsecongeo.75.5.684

Rickli, J., Hindshaw, R.S., Leuthold, J., Wadham, J.L., Burton, K.W., Vance, D., 2017. Impact of glacial activity on the weathering of Hf isotopes – Observations from Southwest Greenland. Geochim. Cosmochim. Acta 215, 295–316. https://doi.org/10.1016/j.gca.2017.08.005

Schwab, M.S., Hilton, R.G., Raymond, P.A., Haghipour, N., Amos, E., Tank, S.E., Holmes, R.M., Tipper, E.T., Eglinton, T.I., 2020. An Abrupt Aging of Dissolved Organic Carbon in Large Arctic Rivers. Geophys. Res. Lett. 47, e2020GL088823. https://doi.org/10.1029/2020GL088823

Tachikawa, K., Piotrowski, A.M., Bayon, G., 2014. Neodymium associated with foraminiferal carbonate as a recorder of seawater isotopic signatures. Quat. Sci. Rev. 88, 1–13. https://doi.org/10.1016/j.quascirev.2013.12.027

839 Tanaka, T., Togashi, S., Kamioka, H., Amakawa, H., Kagami, H., Hamamoto, T.,
840 Yuhara, M., Orihashi, Y., Yoneda, S., Shimizu, H., Kunimaru, T., Takahashi,
841 K., Yanagi, T., Nakano, T., Fujimaki, H., Shinjo, R., Asahara, Y., Tanimizu, M.,
842 Dragusanu, C., 2000. JNdi-1: a neodymium isotopic reference in consistency
843 with LaJolla neodymium. Chem. Geol. 168, 279–281.
844 https://doi.org/10.1016/S0009-2541(00)00198-4
845 Tank, S.E., Striegl, R.G., McClelland, J.W., Kokelj, S.V., 2016. Multi-decadal
846 increases in dissolved organic carbon and alkalinity flux from the Mackenzie
847 drainage basin to the Arctic Ocean. Environ. Res. Lett. 11, 054015.
848 https://doi.org/10.1088/1748-9326/11/5/054015
849 Tipper, E.T., Stevenson, E.I., Alcock, V., Knight, A.C.G., Baronas, J.J., Hilton, R.G.,
850 Bickle, M.J., Larkin, C.S., Feng, L., Relph, K.E., Hughes, G., 2021. Global
851 silicate weathering flux overestimated because of sediment–water cation
852 exchange. Proc. Natl. Acad. Sci. 118.
853 https://doi.org/10.1073/pnas.2016430118
854 Vincent, E., Berger, W.H., 1985. Carbon Dioxide and Polar Cooling in the Miocene:
855 The Monterey Hypothesis, in: The Carbon Cycle and Atmospheric CO2:
856 Natural Variations Archean to Present. American Geophysical Union (AGU),
857 pp. 455–468. https://doi.org/10.1029/GM032p0455
858 Vonk, J.E., Giosan, L., Blusztajn, J., Montlucon, D., Graf Pannatier, E., McIntyre, C.,
859 Wacker, L., Macdonald, R.W., Yunker, M.B., Eglinton, T.I., 2015. Spatial
860 variations in geochemical characteristics of the modern Mackenzie Delta
861 sedimentary system. Geochim. Cosmochim. Acta 171, 100–120.
862 https://doi.org/10.1016/j.gca.2015.08.005

Vonk, J.E., Tank, S.E., Walvoord, M.A., 2019. Integrating hydrology and biogeochemistry across frozen landscapes. Nat. Commun. 10, 5377. https://doi.org/10.1038/s41467-019-13361-5

Walker, J.C.G., Hays, P.B., Kasting, J.F., 1981. A negative feedback mechanism for the long-term stabilization of Earth's surface temperature. J. Geophys. Res. Oceans 86, 9776–9782. https://doi.org/10.1029/JC086iC10p09776

Wheeler, J.O., Hoffman, P.F., Card, K.D., Davidson, A., Sanford, B.V., Okulitch, A.V., Roest, W.R., 1996. Geological map of Canada / Carte géologique du Canada. Geol. Surv. Can. Nat. Resour. Can. https://doi.org/10.4095/208175

Zimmermann, B., Porcelli, D., Frank, M., Andersson, P.S., Baskaran, M., Lee, D.-C., Halliday, A.N., 2009. Hafnium isotopes in Arctic Ocean water. Geochim. Cosmochim. Acta 73, 3218–3233. https://doi.org/10.1016/j.gca.2009.02.028

Zolkos, S., Tank, S.E., Kokelj, S.V., 2018. Mineral Weathering and the Permafrost Carbon-Climate Feedback. Geophys. Res. Lett. 45, 9623–9632. https://doi.org/10.1029/2018GL078748

Figure Captions

Figure 1. Area of study **A.** Sample locations and elevation (GDEM, resolution 30 Arc second). **B**. Bedrock geology of the Mackenzie Basin (shaded black line), categorized by rock type (Wheeler et al., 1996).White circles indicate the location of sampling sites identified in A.

Figure 2. Water discharge from the Mackenzie River (2017 and 2018). Daily discharge (lines) from Environment Canada gauging station at Tsiigehtchic, retrieved from the ArcticGro database (https://www.arcticrivers.org/data, Supplementary text S2). ADCP Discharge at the Middle Channel and Tsiigehtchic (this study, light blue, 2017, dark blue 2018).

Figure 3. εNd on coupled HH leachates (circles), dissolved (<0.2μm only shown) and silicate residue sediment (triangles) at all sampling localities (2017 and 2018). Probability density of sediment residue (green) and leachate (pink) shown, difference in modes (dashed grey line) is indicated (black arrow). Open symbols are bank sediment and coloured symbols, SPM, coloured diamonds are sediment core data. Coloured squares are a shale fragment HH leachate and residue (pink and green respectively), which was not used in the linear regression. Error bars are 2σ analytical uncertainty (where visible or smaller than the symbol size). 1:1 line (dashed line) is shown.

Figure 4. Two sediment depth profiles from the Mackenzie River (Middle Channel, 2017). Water depth is normalised to the deepest sample. Error bars are 2σ analytical uncertainty. Dissolved compositions are from waters obtained at the surface and at depth.

Figure 5. Probability density of the fraction of a suite of elements in leachates relative to the total (sum of leachates and residue). Data is from all sampling sites across both years. The fraction of the HH leachate, acetic acid leachate, and the

sum of all leaching steps are shown. Symbols are data points that form the probability distribution.

Figure 6. Characterisation of sequential extractions A. MREE/MREE* HREE/LREE cross-plot, following Martin et al., 2010, alongside a non-exhaustive literature compilation (plotted for reference, Supplementary Text S2). HREE= Σ(Tm, Yb, Lu) LREE= Σ(La, Pr, Nd), MREE= Σ(Gd, Tb, Dy), MREE*=(HREE+LREE)/2. All concentrations are normalised to PAAS (after Pourmand et al., 2012). Foraminiferal coatings and marine leachates are extractions thought to represent Fe-Mn oxyhydroxides. **B.** A REE partitioning in a Mackenzie (Middle Channel, 2017) SPM sequential extraction. Left hand side axis is the REE concentration, right hand side axis fraction of total (sum of leachates and residue) REE concentration (bars) in each phase. **C.** $^{87}Sr/^{86}Sr$ against εNd on Mackenzie (Middle Channel, 2017) SPM sequential extractions and water ($^{87}Sr/^{86}Sr$ data point from Tipper et al., 2021). 2σ analytical uncertainty is shown, unless smaller than the symbol size.

Figure 7. Schematic indicating the mechanisms presented herein that may lead to more radiogenic εNd in the HH leachates of SPM and the dissolved load of the Mackenzie river, when compared to the SPM silicate residue.

Figure 8. Probability density of calculated $f_{Nd,auth}$ (equation 1) for 4 sampling sites generated using Monte Carlo methods. Median value (white line) and interquartile range (dashed lines) are shown. Input compositions for this calculation are listed in Table S13.

Figure

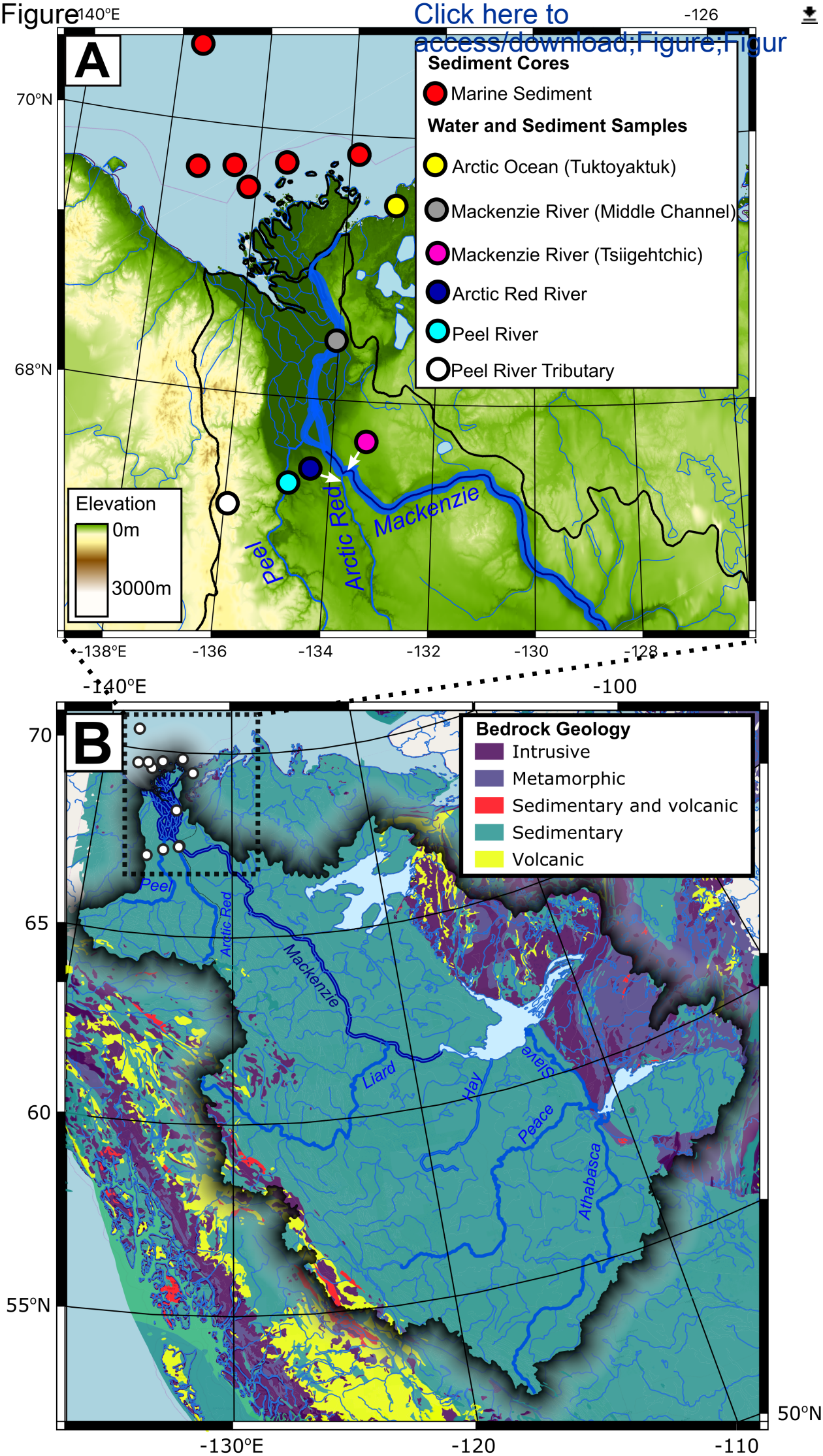

Figure

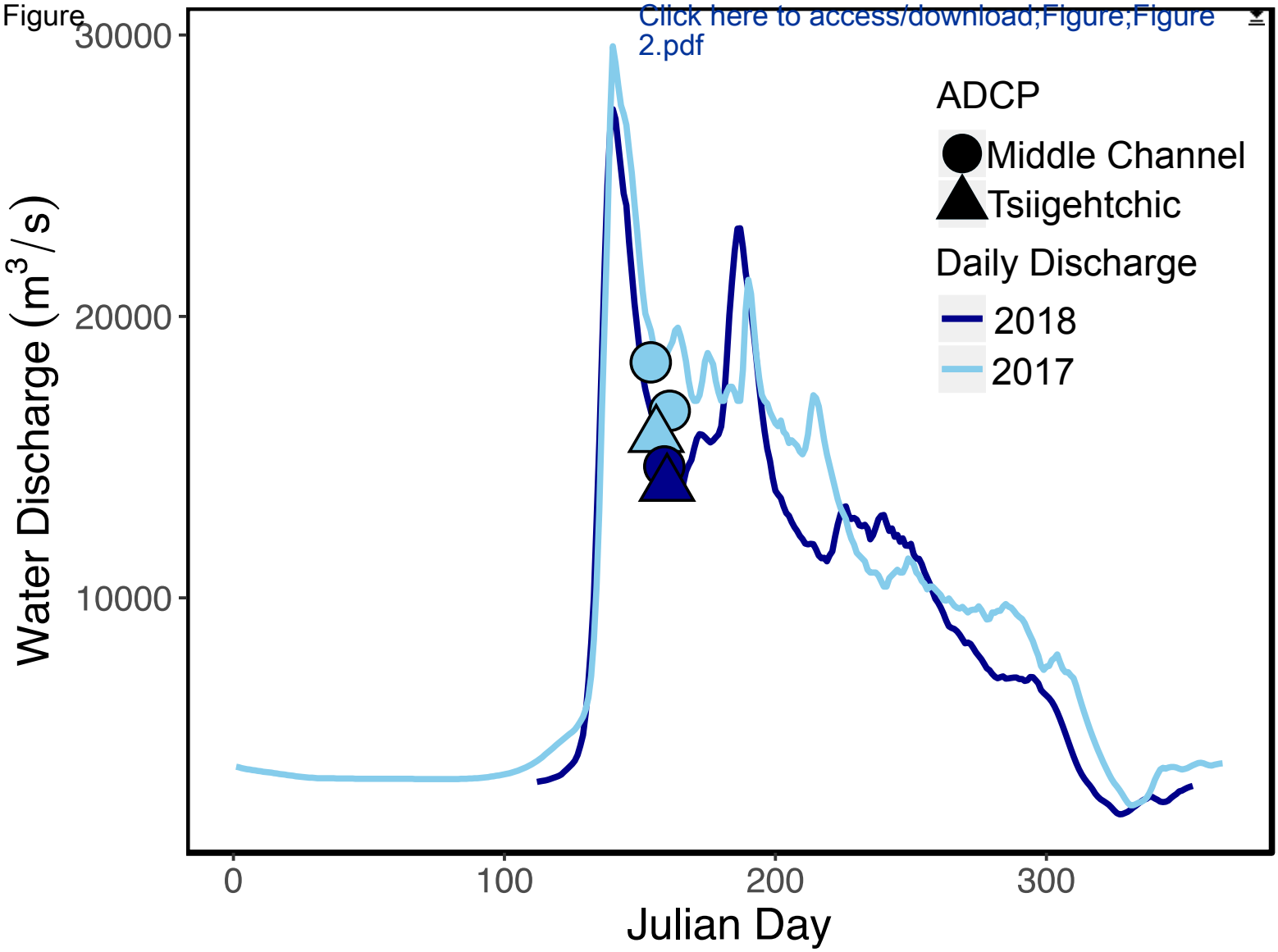
Click here to access/download;Figure;Figure 2.pdf
ADCP
Middle Channel
Tsiigehtchic
Daily Discharge
2018
2017
Water Discharge (m3/s)
30000
20000
10000
0
100
200
300
Julian Day

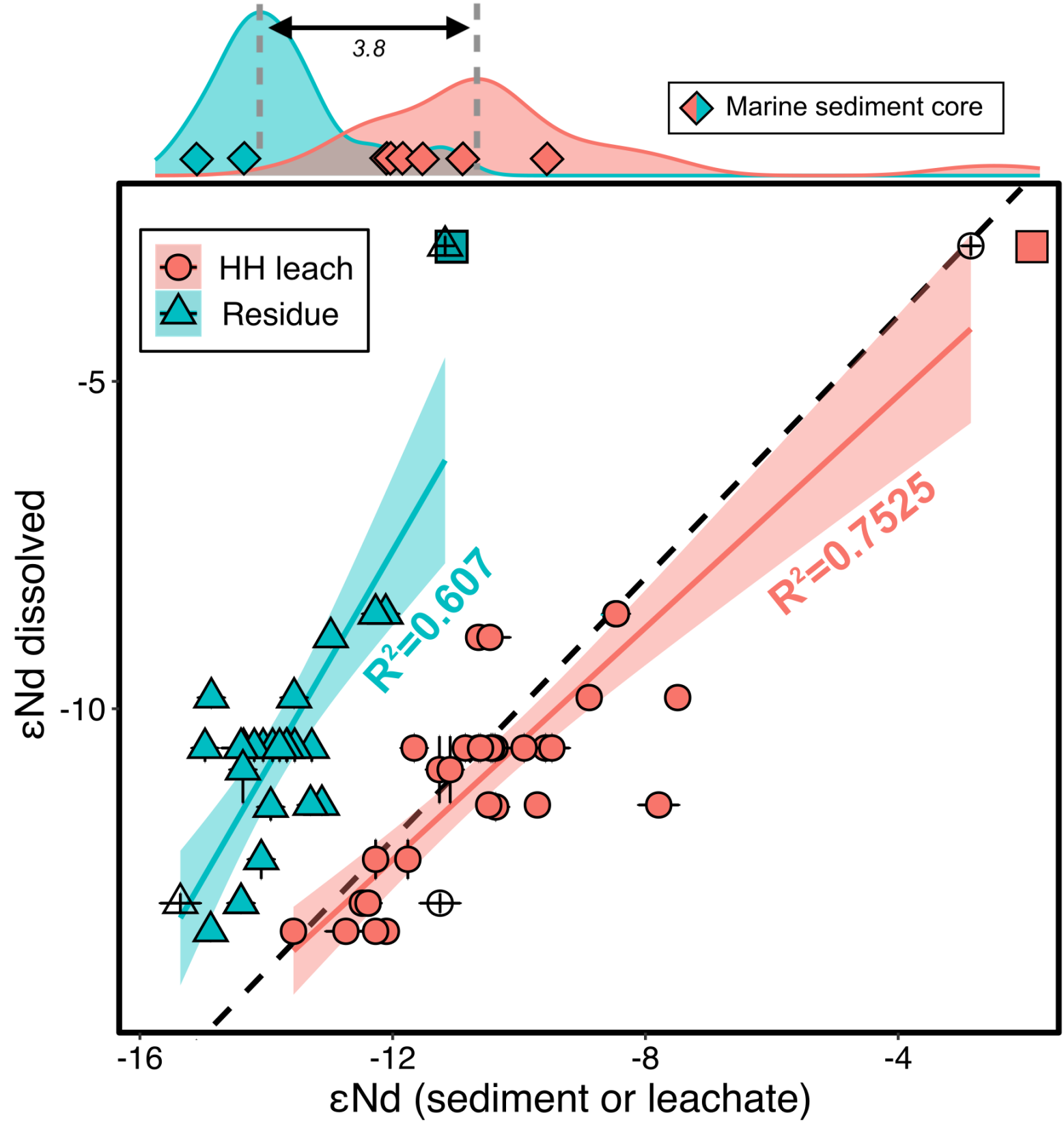
3.8
Marine sediment core
HH leach
Residue
R²=0.607
R²=0.7525
-5
-10
-16
-12
-8
-4
εNd dissolved
εNd (sediment or leachate)

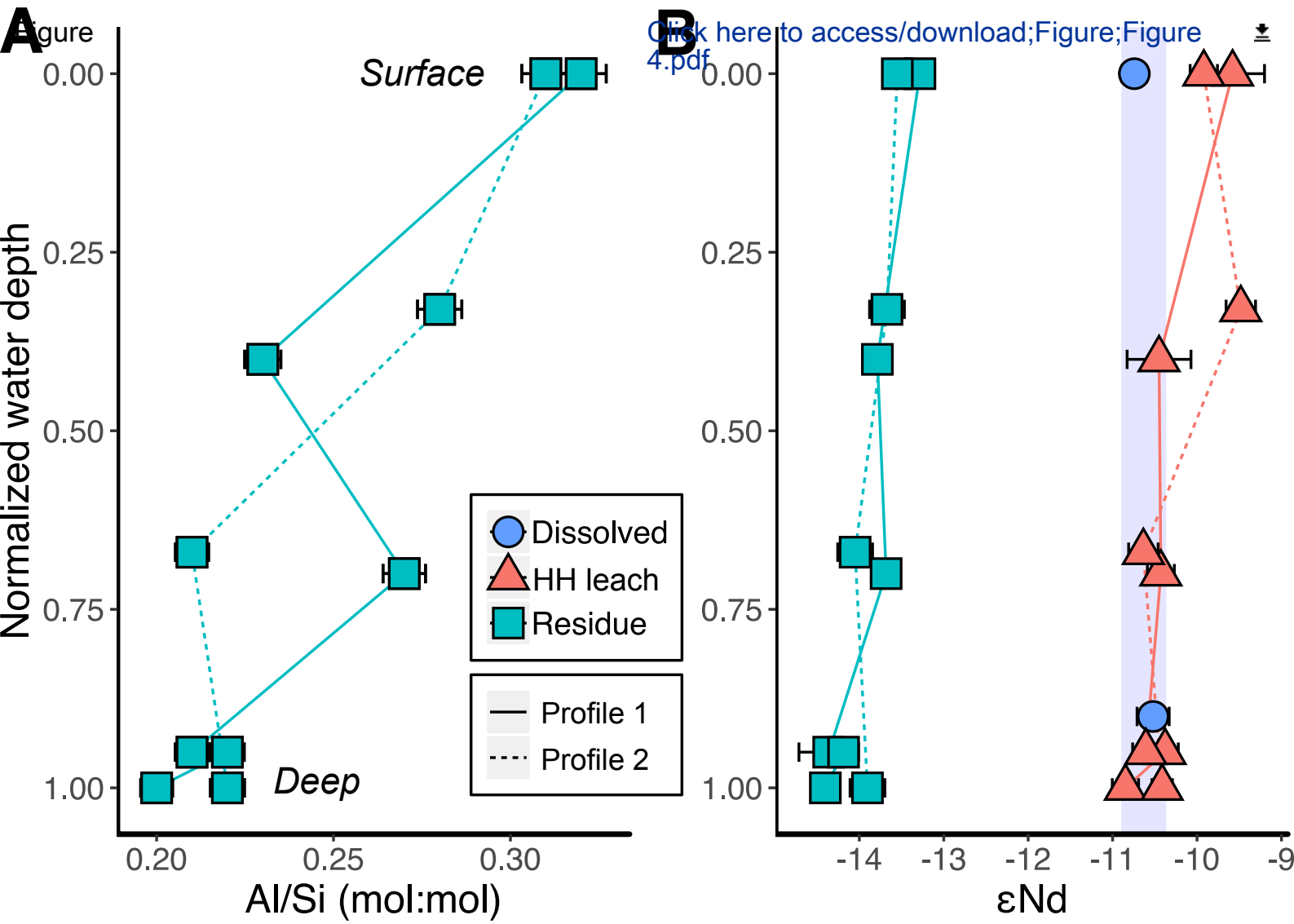

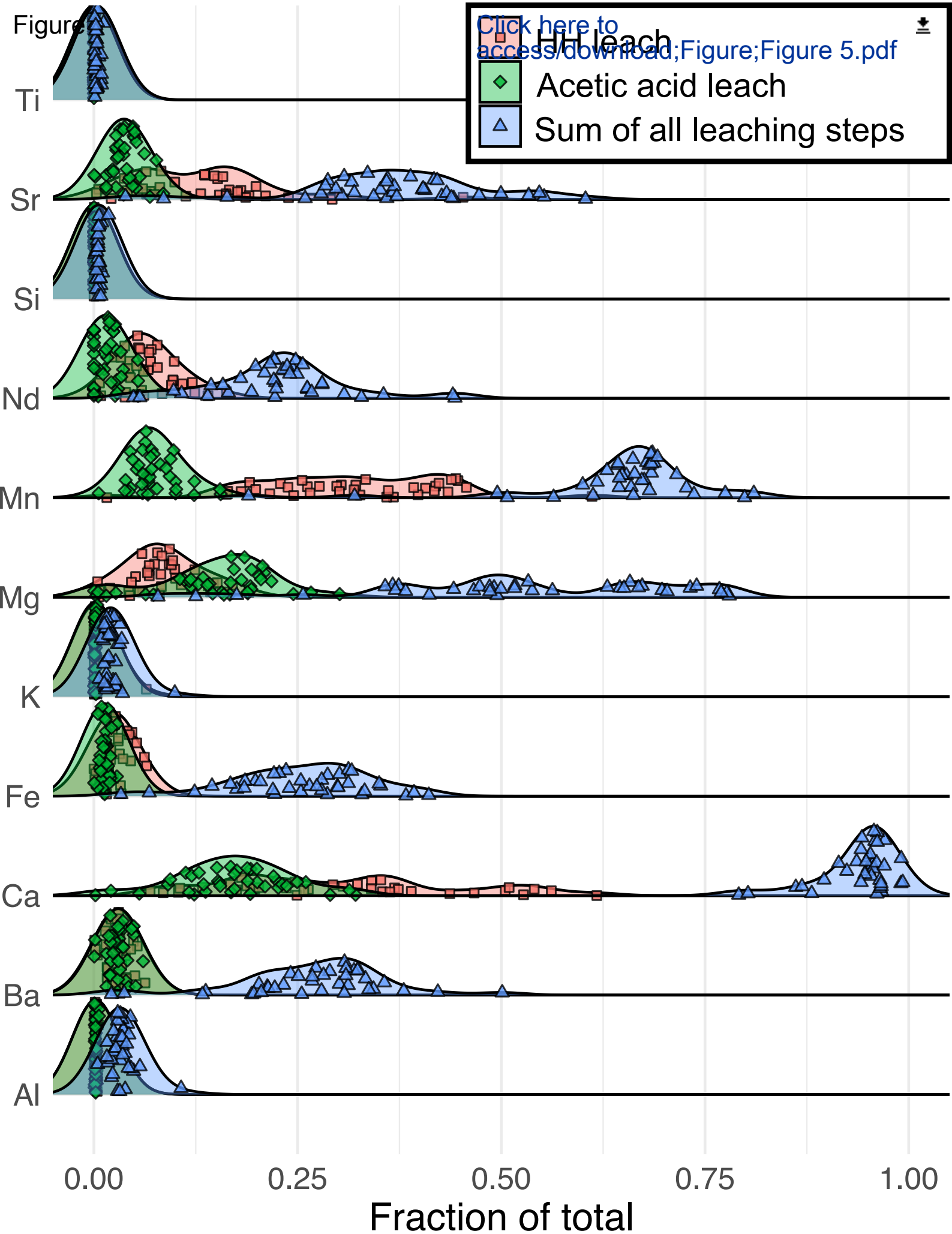
Figure
Click here to access/download;Figure;Figure 5.pdf
HH leach
Acetic acid leach
Sum of all leaching steps
Ti
Sr
Si
Nd
Mn
Mg
K
Fe
Ca
Ba
Al
0.00
0.25
0.50
0.75
1.00
Fraction of total

Figure

Click here to access/download;Figure;Figure 6.pdf

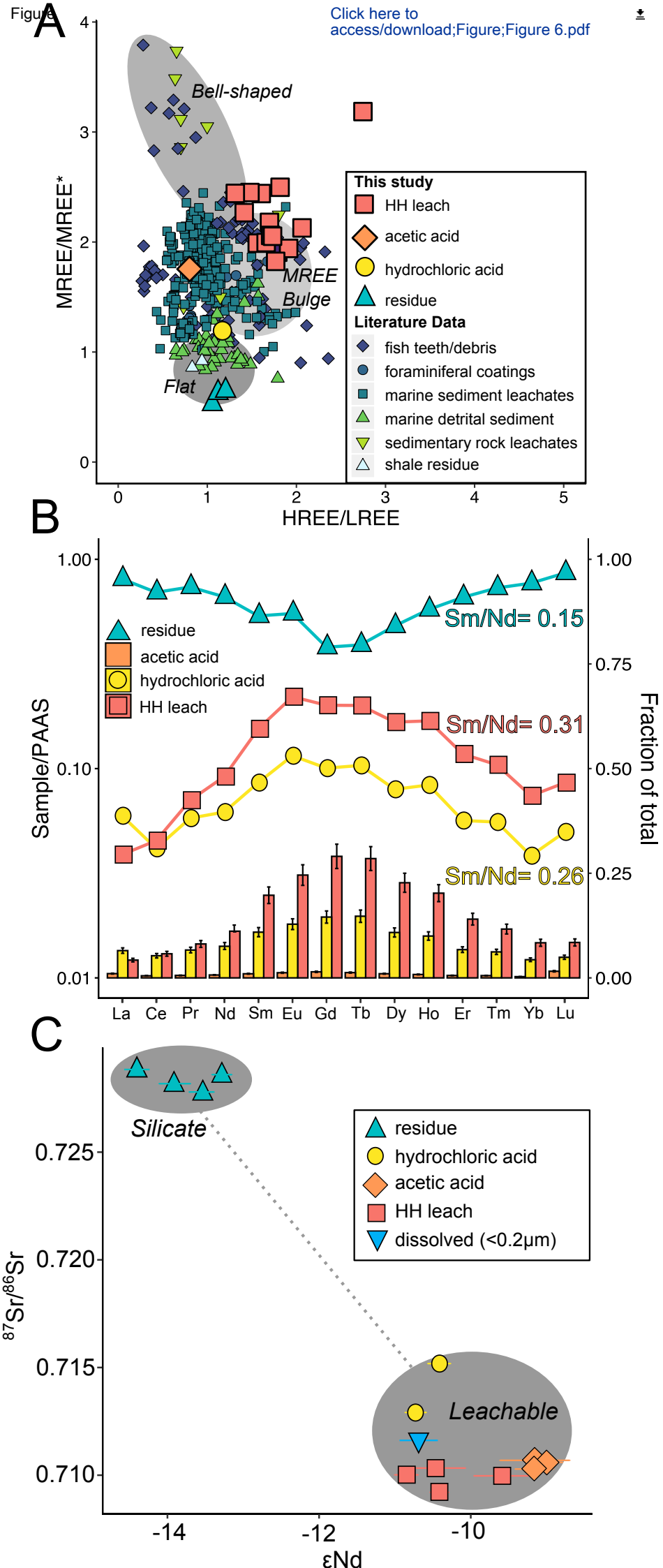

Figure

Click here to access/download;Figure;Figure 8.pdf

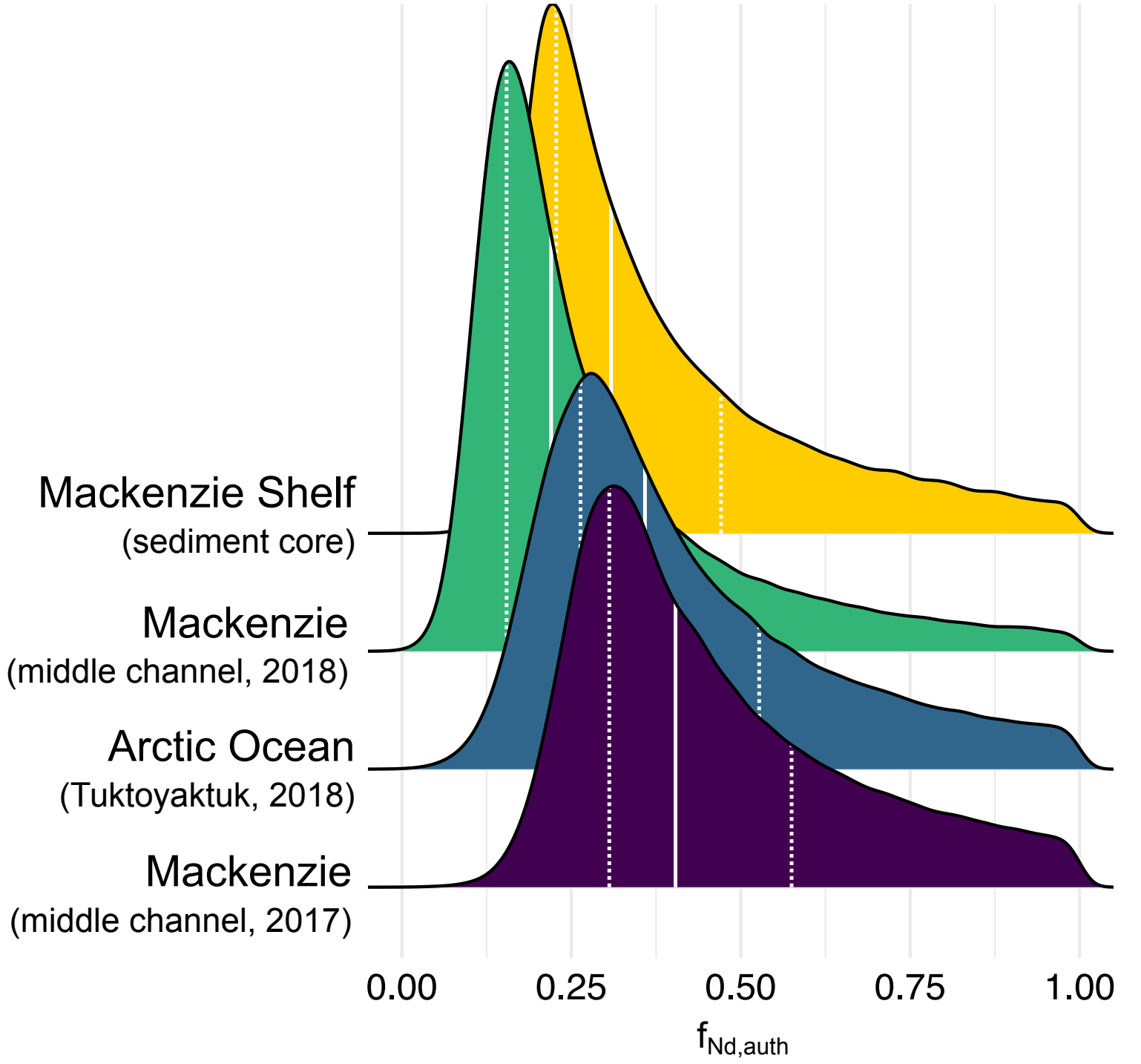

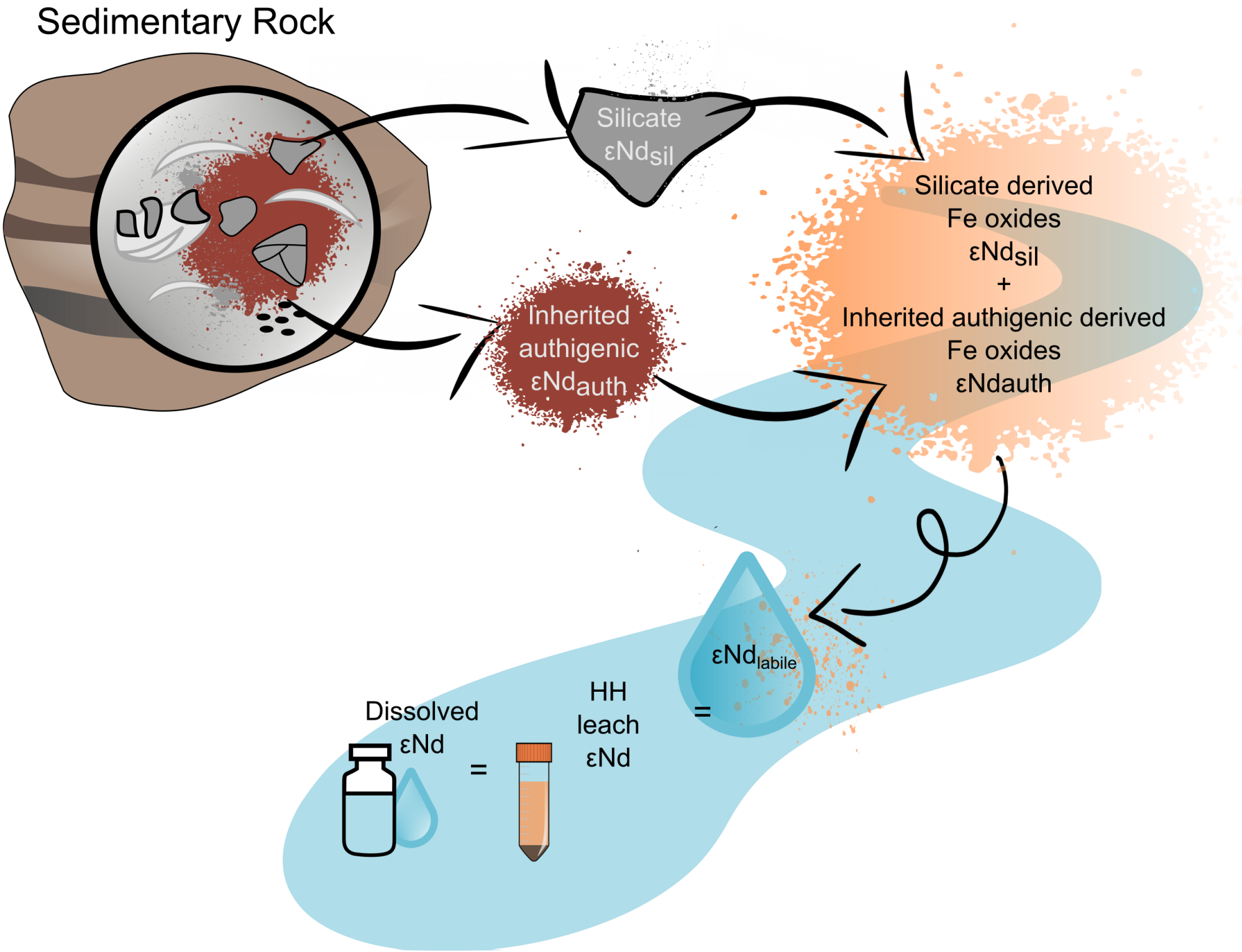
Sedimentary Rock
Silicate
εNdsil
Inherited
authigenic
εNdauth
Silicate derived
Fe oxides
εNdsil
+
Inherited authigenic derived
Fe oxides
εNdauth
εNdlabile
=
Dissolved
εNd
=
HH
leach
εNd

Table 1. εNd and Nd concentrations on different filtrates from the Mackenzie River and a major tributary (2018).

River	Filter Size/MWCO	εNd	Error (2σ)[1]	[Nd] ppt	Error (2σ)	% of <0.2µm
Mackenzie River (Middle Channel)	<0.2µm	-12.97	0.15	20.7[2]	0.7 (n=2)	
	10kda	-12.41	0.51	10.4[3]	1.4 (n=2)	50%
	1kda	-13.40	0.34	5.9[3]	0.4 (n=2)	29%
Peel River	<0.2µm	-11.47	0.15	12.1	n/a (n=1)	
	10kda	-11.61	0.34	7.1[2]	0.1 (n=2)	59%
	1kda	n.d	n.d	4.1[3]	0.8 (n=2)	34%

[1]Analytical uncertainty, [2]Average and 2σ of two replicate measurements during different analytical sessions, [3]Average and 2σ of two full procedural replicates (including filtration)

Author contributions

C.S.L, E.T.T., A.M.P, R.G.H and R.S.H designed the study. C.S.L, R.G.H, M.D, J.J.B carried out the sample collection and fieldwork. R.G.H and E.T.T and C.S.L obtained funding for fieldwork and analysis. C.S.L and R.W carried out method development to analyse the samples. C.S.L analysed the samples and wrote the manuscript under the supervision of E.T.T and A.M.P with input and guidance from all co-authors.